Mixing and diapycnal advection in the ocean

Louis C. St. Laurent

School of Earth and Ocean Sciences, University of Victoria, Victoria, British Columbia, Canada

John M. Toole and Raymond W. Schmitt

Woods Hole Oceanographic Institution, Woods Hole, Massachusetts, USA

Abstract. In the stratified ocean, vertical motions arise from both adiabatic and diabatic mechanisms. Diapycnal advection is the vertical component of flow across an isopycnal surface which occurs when mixing produces a divergent flux of buoyancy. Buoyancy forcing of the lateral flow by vortex stretching occurs when diapycnal advection rates vary with depth. Microstructure observations of enhanced turbulence above rough topography are presented. These data allow us to distinguish the influence of diabatic forcing on the circulation. Estimates of diapycnal advection are used to quantify the diabatic flow, and the role of diapycnal advection as a mechanism of vortex stretching on the circulation is assessed. The divergence of diapycnal mass flux is found to be a significant forcing mechanism for the circulation occurring above fracture zone topography. Moreover, both the direction and magnitude of diapycnal advection are dependent on the efficiency of turbulence at generating a buoyancy flux. Depth variations of diapycnal advection suggest the mixing efficiency is reduced in weakly stratified abyssal canyons.

Introduction

The sun heats the Earth's atmosphere and ocean, driving the winds, evaporation, and rain. These act over global scales to input mechanical energy and variance to the scalar fields of the ocean. Turbulence acts at the smallest scales of fluid motion, where variance is dissipated by molecular processes. Stirring is the mechanism that acts at the intermediate range of scales, advecting variance both in physical and wavenumber space.

The input of variance at the largest scales is related to the mechanical and buoyancy forcing that drives the so-called "large-scale circulation". However, circulations can be forced by mechanisms occurring anywhere along the variance cascade. For example, *Spall* (1994) describes large-scale abyssal recirculations driven by the eddy fluxes of topographic waves. Examples of eddy driven mean flows are described by *Lozier* (1997) and *Alves and Colin de Verdiere* (1999). Buoyancy forcing may also originate at any scale. In particular, turbulent mixing at the smallest scales of motion can give rise to

divergent fluxes of heat and salt. If the buoyancy forces that result from turbulence are significant relative to other forcing, a large-scale circulation may develop by the direct influence of small-scale mixing. *Spall* (2000) demonstrates that mixing near large-scale topography is particularly effective at driving strong buoyancy-forced circulations.

Stommel (1957) first proposed that the abyssal circulation of the ocean may be driven by buoyancy forcing, and a model proposed by *Stommel and Arons* (1960) described a simple set of dynamics governing the buoyancy driven flow. The Stommel-Arons model is still central to our view of the abyssal circulation problem, and the important role of buoyancy forcing in the abyss is not questioned. However, the nature of deep buoyancy forcing has only recently come to light, with observations providing new insight into the mechanisms driving abyssal circulations. Observations of turbulence across the Brazil Basin show that abyssal mixing rates are spatially nonuniform, with enhanced mixing occurring above regions of rough topography (*Polzin et al.,*

1997). *Ledwell et al.* (2000) and *St. Laurent et al.* (2001) suggest that energy from internal tides sustains the elevated turbulence in these regions.

In the report that follows, the implications for buoyancy forcing by small-scale mixing are discussed. Observations from the abyssal Brazil Basin described by St. Laurent et al. (2001) are summarized here. Estimates of cross-isopycnal motion, termed diapycnal advection, are used to quantify the diabatic flow. The diapycnal advection serves as a primary measure of buoyancy forcing.

Diapycnal advection

We wish to consider the diabatic flow in the ocean interior driven by a divergent buoyancy flux. The equation for buoyancy $(b = -(g/\rho_0)\rho')$ is

$$\frac{\partial b}{\partial t} + \mathbf{u} \cdot \nabla b + wN^2 = -\nabla \cdot \mathbf{F} - \frac{\partial J_b}{\partial z}, \qquad (1)$$

where $\mathbf{u} = (u, v)$ is the lateral flow, $\nabla = (\partial/\partial x, \partial/\partial y)$ is the lateral differential operator, and $(\mathbf{F}, J_b)$ are the lateral and vertical components of buoyancy flux. To distinguish diabatic from adiabatic flow, it is useful to consider the buoyancy budget along a neutral surface. Along a neutral surface whose depth is described by $z_i(x, y, t)$, buoyancy is subject to the relations

$$\nabla b_i = \nabla b + \nabla z_i N^2 = 0,$$
$$\frac{\partial b_i}{\partial t} = \frac{\partial b}{\partial t} + \frac{\partial z_i}{\partial t}N^2 = 0, \qquad (2)$$

where $(\cdot)_i$ denotes an isopycnal function of (x, y, t), and $N^2 = \partial b/\partial z$. Additionally, since buoyancy flux across an isopycnal occurs only by small-scale turbulence, all fluxes may be expressed in terms of a turbulent diffusivity k_ρ such that

$$\mathbf{F_i} = -k_\rho \nabla b_i = -k_\rho \nabla b - k_\rho \nabla z_i N^2 = 0,$$
$$J_b = -k_\rho N^2. \qquad (3)$$

Thus, the equation for buoyancy on a neutral surface can be expressed as

$$\left(w - \frac{\partial z_i}{\partial t} - \mathbf{u} \cdot \nabla z_i\right)N^2 = \frac{\partial(k_\rho N^2)}{\partial z} - \nabla \cdot \left(k_\rho \nabla z_i N^2\right). \qquad (4)$$

We define the vertical advection quantity $w_* = w - \partial z_i/\partial t - \mathbf{u} \cdot \nabla z_i$ as the "diapycnal advection". As discussed by *McDougall* (1987, 1995) and *Pedlosky* (1996),
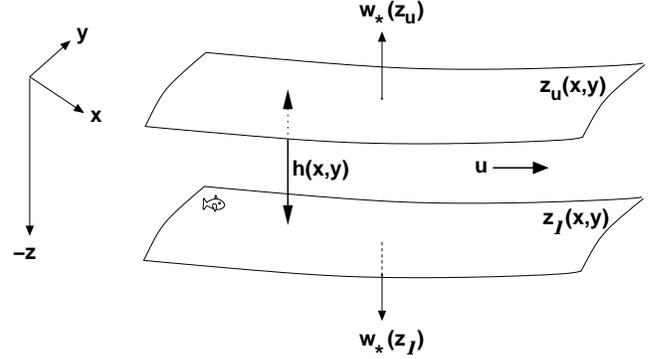
Figure 1. Diagram showing the parameters of a steady-state density layer.

w_* is the vertical component of flow through (not normal to) isopycnals, and is the vertical motion that is caused by a divergent buoyancy flux. The divergent buoyancy flux is comprised of two terms; a standard vertical divergence term $-\partial J_b/\partial z$, and a lateral divergence of vertical buoyancy flux $\nabla \cdot (\nabla z_i J_b)$. It is useful to consider the ratio of these terms, with scaling $\partial J_b/\partial z \sim \delta^{-1}J_b$, and $\nabla \cdot (\nabla z_i J_b) \sim \ell^{-2}\delta J_b$ for characteristic lateral and vertical scales (ℓ, δ). The ratio of the vertical to lateral divergence terms is $(\ell/\delta)^2$. In general, we will assume that the aspect ratio δ/ℓ of isopycnals is small, such that $(\ell/\delta)^2 \gg 1$, and (4) can be approximated as

$$w_*N^2 \cong -\frac{\partial J_b}{\partial z}. \qquad (5)$$

Dynamical Considerations

Consider a large-scale geostrophic and inviscid flow. The potential-vorticity equation for flow in a steady-state density layer (Fig. 1) is

$$\beta v = \frac{f}{h}\mathbf{u} \cdot \nabla h + \frac{f}{h}\left(w_*(z_u) - w_*(z_l)\right), \qquad (6)$$

where $h(x, y)$ is the thickness of the density layer, and (z_u, z_l) denote the upper and lower bounding isopycnal surfaces. The above expression is the density-layered version of the *Stommel and Schott* (1977) beta-spiral equation, and is discussed by *McDougall* (1988) and *Hautala and Riser* (1993). In (6), the advection of planetary vorticity is balanced by vortex stretching. Vortex stretching may occur adiabatically by flow along sloping isopycnals, or diabatically by the divergence of diapycnal advection. Diabatic vortex stretching is related to

the divergence of buoyancy flux by (5). During mixing events, vertical exchanges of buoyancy are accompanied by dissipation of turbulent kinetic energy (TKE), and the energy budget for an ensemble of turbulent events is

$$(1 - R_f)J_b + R_f \overline{\epsilon} = 0, \qquad (7)$$

where ϵ is the dissipation rate, and R_f is the efficiency of the mixing. The TKE budget expressed in (7) assumes steady-state and homogeneous statistics of the Reynolds stress tensor. This equation is discussed by Osborn (1980), and an expression for the eddy diffusivity is readily derived by substituting $J_b = -k_\rho N^2$ into (7),

$$k_\rho = \left(\frac{R_f}{1 - R_f}\right)\left(\frac{\overline{\epsilon}}{N^2}\right). \qquad (8)$$

The fraction $\Gamma = R_f(1 - R_f)^{-1}$ (equivalently $\Gamma = -J_b/\overline{\epsilon}$), the ratio of buoyancy flux to energy dissipated, is typically taken to be $\leq 20\%$ for stratified turbulence. With use of (5) and (7), the diapycnal advection can be expressed as

$$w_* \cong N^{-2}\frac{\partial(\Gamma\overline{\epsilon})}{\partial z}, \qquad (9)$$

and the potential vorticity equation (6) can be expressed as

$$\beta v = \frac{f}{h}\mathbf{u} \cdot \nabla h + \frac{\partial}{\partial z}\left(\frac{f}{N^2}\frac{\partial(\Gamma\overline{\epsilon})}{\partial z}\right), \qquad (10)$$

where we have taken $(w_*(z_u) - w_*(z_l))/h = \partial w_*/\partial z$.

As a clear way of demonstrating the importance of the diabatic forcing term in (10), it is useful to consider the following scaling relations. Using standard notation, we scale $(\mathbf{x}, z) \sim (L, H)$, $\mathbf{u} \sim U$, $\beta \sim U/L^2$ and define the deformation radius as $R_d = NH/f$. The scaling for the term ∇h is taken from the geostrophic relation $fU \sim g'\nabla h$, where the reduced gravity is $g' \sim N^2 H$. Additionally, we scale the energy dissipation term as $\epsilon \sim fE$, where E is the scale of the kinetic energy associated with the forcing for the vertical mixing. This scaling for ϵ is proposed on solely dimensional grounds, noting that a time scale f^{-1} is relevant for many dynamical regimes. Application of these scaling relations in (10) yields the following nondimensional equation,

$$\beta v = \frac{L^2}{R_d^2}\mathbf{u} \cdot \frac{\nabla h}{h} + \frac{E}{U^2}\frac{\partial}{\partial z}\left(\frac{L^2}{R_d^2}\frac{\partial(\Gamma\overline{\epsilon})}{\partial z}\right), \qquad (11)$$

where the lower-case variables are now dimensionless. The ratio of the diabatic to adiabatic stretching is

$$\frac{\text{diabatic stretching}}{\text{adiabatic stretching}} = \Gamma\frac{E}{U^2}. \qquad (12)$$

The relative importance of the diabatic-forcing term will be set by the energy level of the process controlling the vertical mixing. In the case of dissipating internal-tide energy, the energy flux scales as U_{tide}^2. In the abyss where geostrophic flow is weak, typical geostrophic velocities are $U \sim 5$ mm s^{-1}, while tidal velocities are generally $U_{\text{tide}} \sim 20$ mm s^{-1}. Thus a ratio of O(1) for the diabatic to adiabatic vorticity forcing is easy to justify, demonstrating the strong dynamical link between mixing and circulation in the abyss.

## Observations of turbulence in the Abyssal Brazil Basin

In the period between January 1996 and April 1997, two microstructure surveys were made in the Brazil Basin. The 1996 survey consisted of a basin-scale survey and the initiation of a tracer dispersion experiment at a site near the Mid Atlantic Ridge (MAR). During the 1997 survey, a detailed survey was conducted over a 5×10^5 km^2 region of rough topography near the tracer release site. The primary focus of the 1996 survey was the spatial variability of mixing levels, and a report on the observed variability is given by *Polzin et al.* (1997). Results from the tracer release experiment are described by *Ledwell et al.* (2000).

The presentation here will focus on the dissipation data collected over the fracture zone (FZ) topography near the MAR (Fig. 2). All profiles consist of conventional hydrographic variables (e.g., Θ, S, U, V) in addition to microstructure, and generally extend from the surface mixed layer to within 20 m of the bottom. The bathymetric data shown in Fig. 2 were derived from satellite measurements of the marine gravity field *Smith and Sandwell* (1997). The map clearly shows the network of FZs leading east to the MAR. This system of FZs is characterized by a series of canyons bounded latitudinally by crests that rise up to 1 km above the canyon floors.

Turbulent kinetic energy dissipation rates were derived from observations of velocity microstructure. Only two components of the strain tensor are measured, and isotropy is assumed to express the dissipation rate as $\epsilon = (15/4)\cdot (<u_z^2> + <v_z^2>)$. A summary of the observed deep-dissipation data was made by collapsing the latitudinal spread of the profiles (Fig. 3).
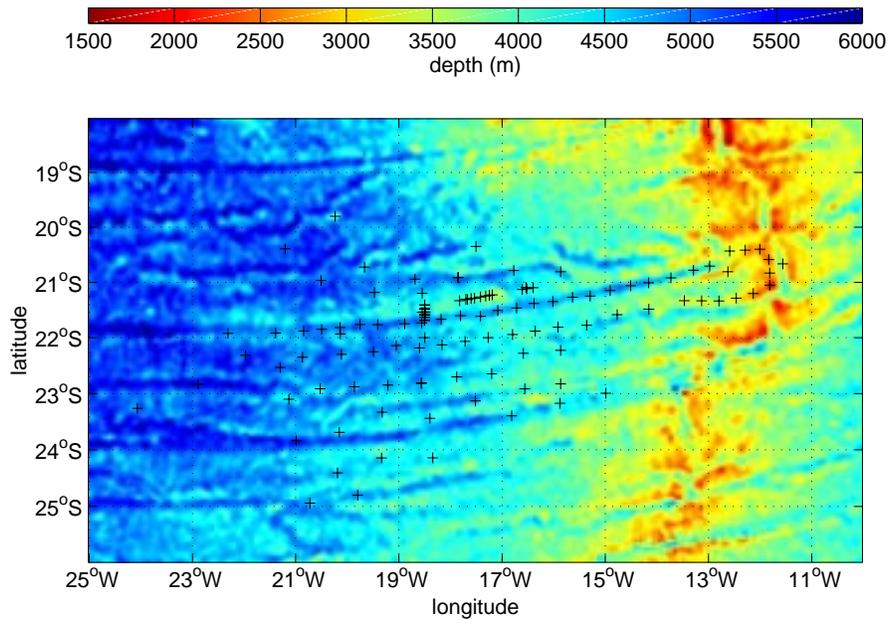
Figure 2. Map of the 1997 survey site with the 2 arc-minute resolution bathymetric estimates of /it Smith and Sandwell (1997). A total of 129 profiles of dissipation rate observations (crosses) were collected in this region.
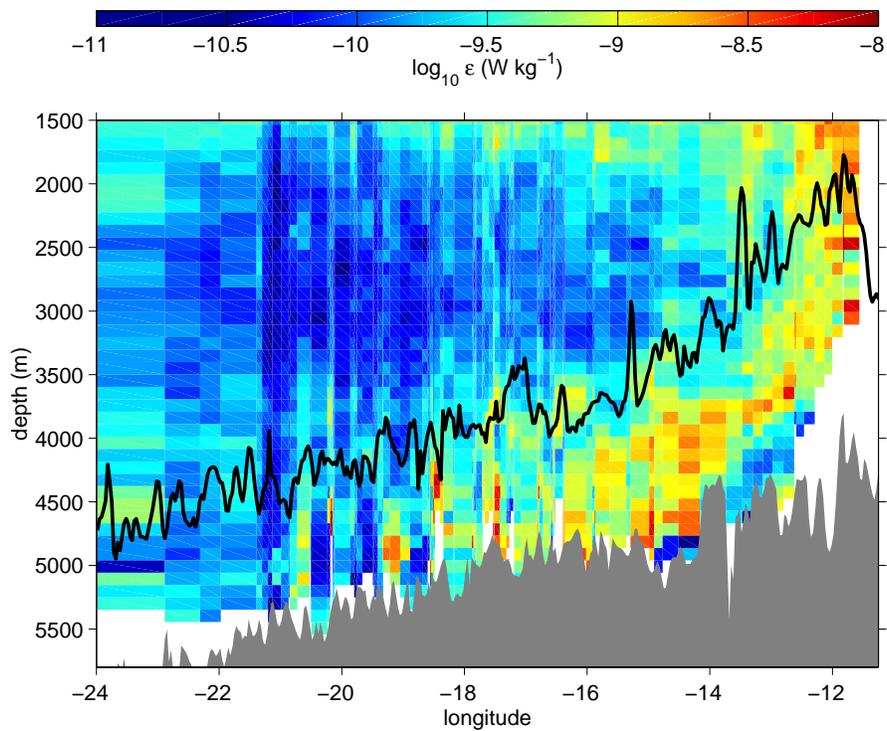
Figure 3. A zonal section of TKE dissipation rate ϵ. The individual profiles are shown as columns, and dissipation rate observations were vertically averaged into 100 m-bins. The shaded bathymetry is representative of canyon floors, while the shallower trace represents the level of ridge crests.

To simplify the presentation, only the depth range deeper than 1500 m is shown. The dissipation data were depth averaged into 100-m intervals, and individual profiles are shown as columns of binned dissipation. Since the latitudinal extent of the survey has been collapsed, no particular section of bathymetry is entirely appropriate. Instead, two classes of representative bathymetry are shown: the bathymetry of FZ crests and the bathymetry of canyon floors, as sampled from the latitude range 21°S to 23°S. Within about 500 m of the bottom, there is an enhancement of dissipation by more than two orders of magnitude over values observed at mid depth. Enhanced dissipation generally occurs between the level of FZ crests and canyon floors, suggesting the largest mixing rates occur in canyons.

An inverse estimate of circulation

Surveyed hydrography was used to divide the flow regime into a series of density layers. In these layers, geostrophic advection is related to isobaric gradients of geopotential anomaly (φ) by

$$\mathbf{u} = \hat{z} \times \frac{\nabla \varphi}{f} + \mathbf{u_0}, \tag{13}$$

where $\mathbf{u_0}$ is a reference level velocity. Thus, the advection of potential vorticity through a density layer of thickness $h(x, y)$, as previously stated in (6), may be expressed in the form

$$\frac{h_x}{h}u_0 + \left(\frac{h_y}{h} - \frac{\beta}{f}\right)v_0 \quad + \quad \frac{1}{h}\left(w_*(z_u) - w_*(z_l)\right)$$
$$= \quad -u_r\frac{h_x}{h} - v_r\left(\frac{h_y}{h} - \frac{\beta}{f}\right), \tag{14}$$

where (u_r, v_r) are the components of relative geostrophic velocity given by $(u - u_0, v - v_0)$ in (13). Thus, the problem of determining the lateral flow $\mathbf{u}$ is reduced to determining the reference level velocity, i.e., the vertical integration constants (u_0, v_0) of a thermal-wind balance.

In layers where flow encounters topography, the use of the geostrophic balance is questionable. A modified momentum balance, such as that of the bottom Ekman layer, may be called for in regions where a density layer comes within O(100) m of the bottom. Additionally, the difficulty of defining the geopotential anomaly along pressure surfaces interrupted by bathymetry severely limits the practical use of (13) and (14) in deep layers. For these reasons, it is necessary to employ additional dynamical constraints on the flow. This is
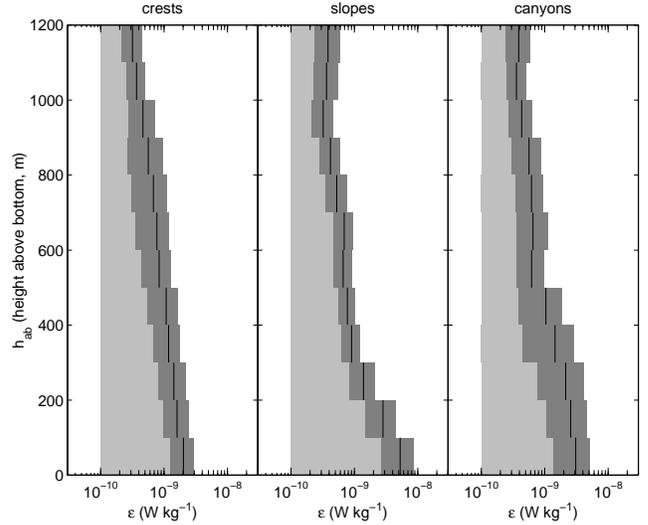
Figure 4. Dissipation profiles averaged according to bathymetric classification. Bathymetric classes were assigned as crests, canyons, or slopes. All profiles are shown relative to a reference dissipation of $\epsilon = 1 \times 10^{-10}$ W kg^{-1}. The 95% confidence interval is shown for each 100-m average.

achieved through the use of integrated advective budgets for mass,

$$\iint dy dz\, u|_x^{x+\gamma} \quad + \quad \iint dx dz\, v|_y^{y+\Delta}$$
$$+ \quad \iint dx dy\, w_*|_{z_l}^{z_u} \quad = \quad 0 \tag{15}$$

and for potential temperature

$$\iint dy dz\, u\Theta'|_x^{x+\gamma} \quad + \quad \iint dx dz\, v\Theta'|_y^{y+\Delta}$$
$$+ \quad \iint dx dy\, w_*\Theta'|_{z_l}^{z_u} \quad =$$
$$\iint dy dz\, \kappa\Theta_x|_x^{x+\gamma} \quad + \quad \iint dx dz\, \kappa\Theta_y|_y^{y+\Delta}$$
$$+ \quad \iint dx dy\, k_\rho\Theta_z|_{z_l}^{z_u}. \tag{16}$$

The integrated expressions (15) and (16) are bounded in control volumes of meridional and zonal extent (γ, Δ), and vertically bounded in a density layer by the surfaces $z_u(x, y)$ and $z_l(x, y)$.

Relations for the diapycnal diabatic terms are expressed using the dissipation rate with the use of (8) and (9). For use in the inverse model, the mixing efficiency
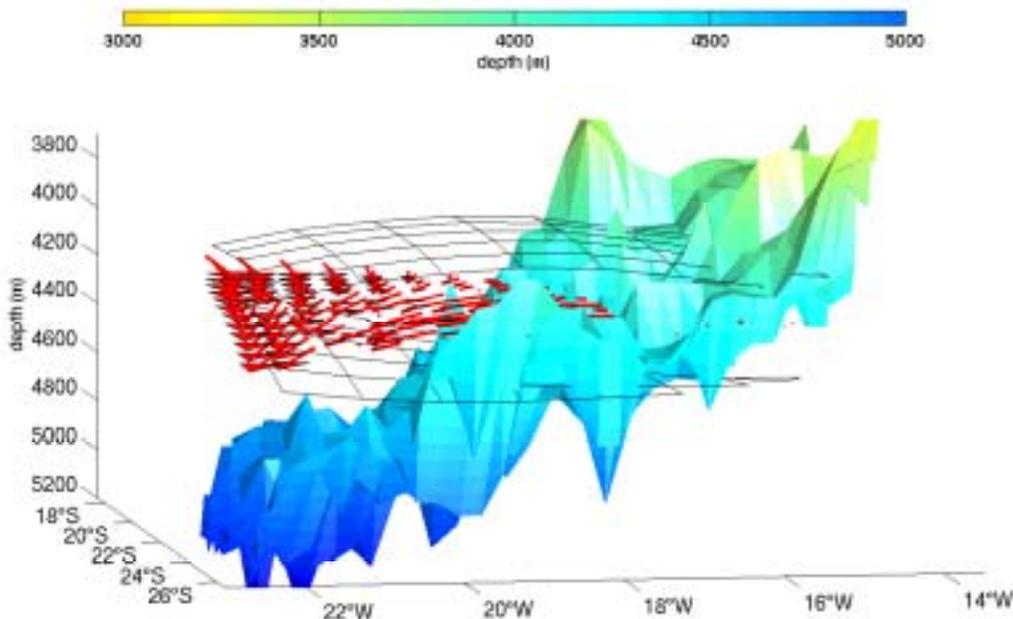
Figure 5. Layer-averaged flow for the density layer $28.16 < \sigma_n < 28.20$. The gridded surfaces show the $\sigma_n = 28.16$ (upper) and $\sigma_n = 28.20$ (lower) isopycnals. Bottom bathymetry was subsampled onto a $0.25° \times 0.25°$ Mercator grid. The largest vectors are (5-6) mm s^{-1}.

parameter Γ is treated as constant, $\Gamma_0 = 0.20 \pm 0.04$. This allows us to specify the diapycnal diffusivity for turbulence as

$$k_\rho \cong \frac{\Gamma_0}{N^2}\overline{\epsilon}, \qquad (17)$$

and the diapycnal advection as

$$w_* \cong \frac{\Gamma_0}{N^2}\frac{\partial\overline{\epsilon}}{\partial z}. \qquad (18)$$

We emphasize that (17) and (18) are approximations, where a constant mixing efficiency has been assumed. While oceanic observations of turbulence from well stratified regions suggest $\Gamma_0 \cong 0.2$ (*Moum*, 1996; *St. Laurent and Schmitt*, 1999), observations from fjords suggest $\Gamma \cong 0.05$ (*Stigebrandt and Aure*, 1989). Additionally, laboratory measurements of turbulence suggest $0.05 < \Gamma < 0.25$ characterizes the variation of mixing efficiency over a wide range Reynolds, Richardson, and Froude numbers (*Ivey and Imberger*, 1991; *Huq and Britter*, 1995). In our inverse model estimates, we accept that using $\Gamma_0 = 0.2 \pm 0.04$ may lead to a specification of k_ρ that is biased high. The use of a constant mixing efficiency in (18) is more problematic, as variations in Γ with depth will not only influence the magnitude of the w_* estimate, but also the sign ($w_* > 0$

for upwelling, $w_* < 0$ for downwelling). For this reason, w_* is regarded as an unknown in the inverse model, and (18) serves as a "constraint" in the inversion. In this manner, (18) provides an a priori estimate, while full inversion of (14), (15), and (16) determines the best estimate of w_*.

In expressions (17) and (18), $\overline{\epsilon}$ is meant to denote some suitably averaged function of the dissipation data. Averaging over multiple profiles is necessary to achieve statistical stability in the mean dissipation estimates. Since our inverse model utilizes the steady-state forms of the advective budgets, we seek an averaging procedure that yields an estimate of the time-mean dissipation rate. Thus, the dissipation data were averaged in both space and time. The time averaging was weighted by a function of the squared barotropic tidal-current speed to remove biases associated with a spring-neap modulation. Furthermore, dissipation data were spatially averaged according to a bathymetric classification scheme. Dissipation profiles above FZ canyons, crests, and the sloping topography between, were treated separately in the averaging. The profile data, classified in this manner, are shown in Fig. 4. Each ensemble profile results from data that has been vertically averaged into 100-m bins. Dissipation decreases with height above
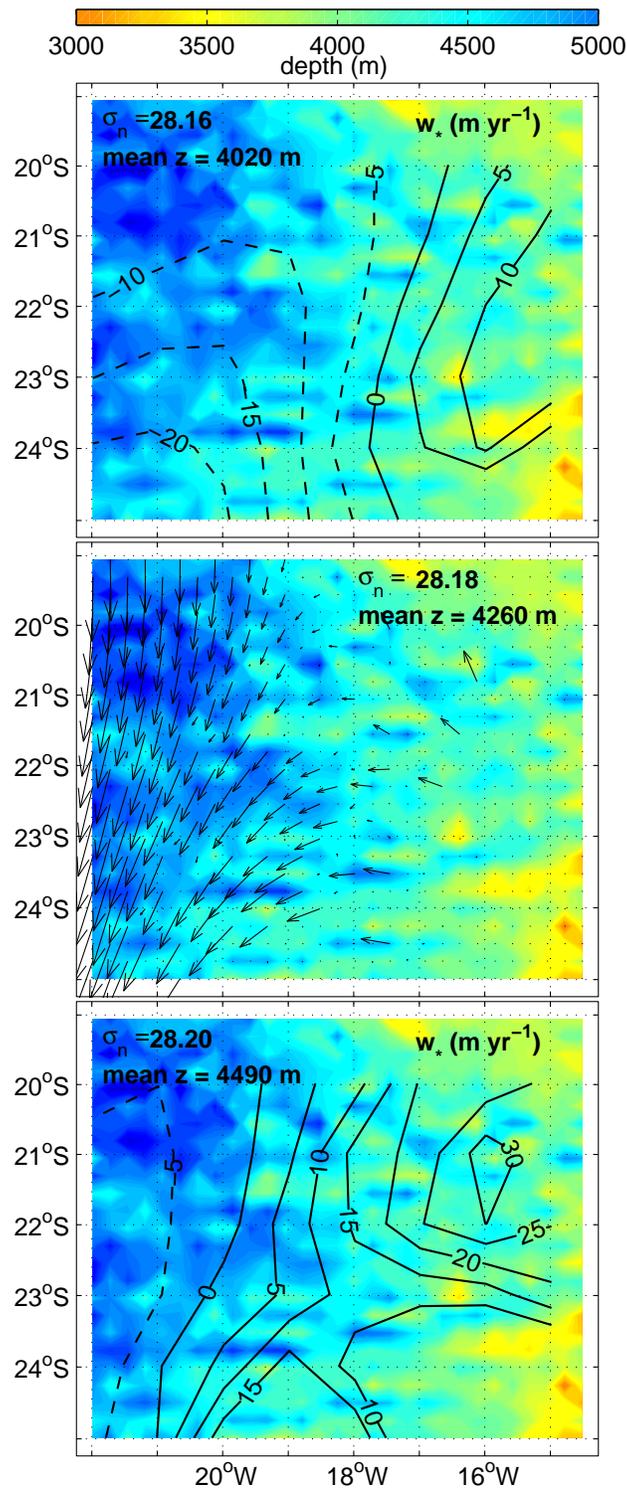
Figure 6. Diapycnal advection estimates for the $\sigma_n = 28.16$ (upper panel) and $\sigma_n = 28.20$ (lower panel) isopycnals. The lateral flow for this density layer (from Fig. 5) is shown in the middle panel. Contoured estimates of diapycnal advection have been averaged over $1° \times 1°$ Mercator cells which include regions blocked by topography.

bottom in each of the 3 classes, and all profiles reach background levels of dissipation, $\epsilon \cong 3 \times 10^{-10}$ W kg^{-1}, at heights greater than 1000 m. The slope profile is notably different from the other two, in both the magnitude of the maximum dissipation and the scale of decay. The slope profile has a bottom value of $\epsilon \cong (3-9) \times 10^{-9}$ W kg^{-1} and decays with an e-fold scale of (150 ± 50) m. The crest and canyon profiles peak at $\epsilon \cong (2-5) \times 10^{-9}$ W kg^{-1} and decay over a larger scale, (500 ± 100) m.

A matrix model for a 6 density layer system consisting of about 7000 equations for 3200 unknowns was formed using (14), (15), (16), (17), and (18). The details of the linear inversion are given by *St. Laurent et al.* (2001). In a series of initial calculations, lateral diffusivity κ was treated as constant along each density surface used in the inversion. Using this approach, the estimates of κ were inconsistent with the a priori estimates of $\kappa \sim 100$ m^2 s^{-1} derived from float observations (*Hogg and Owens*, 1999). Spatial variations of κ on isopycnals intersecting topography may account for this discrepancy. Additionally, diagnostic scaling with $\kappa \sim 100$ m^2 s^{-1} indicated that a primary thermal-advection balance (16) occurs between the terms involving advection (both lateral and vertical) and the vertical diffusion term. Scale estimates suggest that the magnitude of the lateral diffusive flux terms in (16) are less than 10% of the diapycnal diffusive flux of potential temperature. For these reasons, terms involving the lateral diffusivity were dropped from the thermal advection equations, leaving the three dimensional flow field $(\mathbf{u}, \mathrm{w}_*)$ as the model unknowns.

Flow in and above abyssal canyons

Here, we present the estimated circulation in and above the FZ canyons. A more complete discussion of the circulation at all depths in this region of the Brazil Basin is given by *St. Laurent et al.* (2001). In the layers deeper than 3000 m, bottom bathymetry has a clear influence on the flow dynamics. In particular, proximity to the bottom is the controlling factor for the magnitude of the diabatic forcing. The vertical diffusivity characterizing these layers is $k_\rho \sim 1 \times 10^{-4}$ m^2 s^{-1} or greater, and this corresponds to an increased importance of the diabatic terms in the governing equations. Flow was estimated in the neutral density layer $28.16 < \sigma_n < 28.20$ (Fig. 5). The upper isopycnal for this layer ($\sigma_n = 28.16$) rests just above the level of the FZ crests at 16°W. Near the MAR, there is westward flow out of canyons with average current magnitudes of

(2-4) mm s^{-1}. Further west, the density layer's average height above bottom increases, and flow at 500 m above the level of FZ crests is southward with average current magnitudes of (5-6) mm s^{-1}.

Diapycnal advection estimates are presented in Fig. 6. These contoured fields of w_* have been highly smoothed. Where FZ crest topography intersects each density surface, there is no flow, and the contoured maps show estimates of w_* that have been averaged in $1° \times 1°$ cells which often include regions blocked by topography. The $\sigma_n = 28.16$ and $\sigma_n = 28.20$ isopycnals are characterized by diapycnal downwelling to the west and diapycnal upwelling to the east. Estimates of upward advection in canyons exceed $w_* \cong 30$ m yr^{-1}, and are as large as $w_* \cong 100$ m yr^{-1} in some local regions. Uncertainty estimates for the diapycnal flow are typically less than $\pm 40\%$ of the contoured values.

To produce a clearer summary of the deep circulation in and above canyons, a zonal stream function (ψ) was defined by latitudinally integrating the velocity so that $\overline{u}\delta_y = -\psi_z$ and $\overline{w_*}\delta_y = \psi_x$, where the latitudinal limits of integration were taken over the inverse domain (19°S - 25°S),

$$\overline{u}(x,z) = \tfrac{1}{\int dy} \int dy\, u(x,y,z),$$
$$\overline{w_*}(x,z) = \tfrac{1}{\int dy} \int dy\, w_*(x,y,z). \tag{19}$$

An objective analysis technique was used to interpolate the inverse solution and compute the stream function. The resulting smoothed stream-function is shown in Fig. 7 relative to representative bathymetry and the density field. These estimates suggest eastward flow in canyons. Diapycnal upwelling occurs at sites where isopycnals in-crop along canyon floors, and this upwelling feeds the westward flow at the level of the FZ crests.

Deep upwelling and mixing efficiency

As presented above, strong diapycnal upwelling is required to close the heat and mass budgets in regions where density surfaces intersect canyon floors. Figure 8 presents a comparison of the a priori estimates of w_* to the inverse solutions for w_* on the $\sigma_n = 28.20$ neutral surface. Inverse estimates are generally consistent with the a priori estimates of w_* at sites where the $\sigma_n = 28.20$ surface is more than 300 m above the bottom. However, the inverse estimates suggest diapycnal upwelling is favored at sites where the $\sigma_n = 28.20$ surface is within 300 m of the bottom.
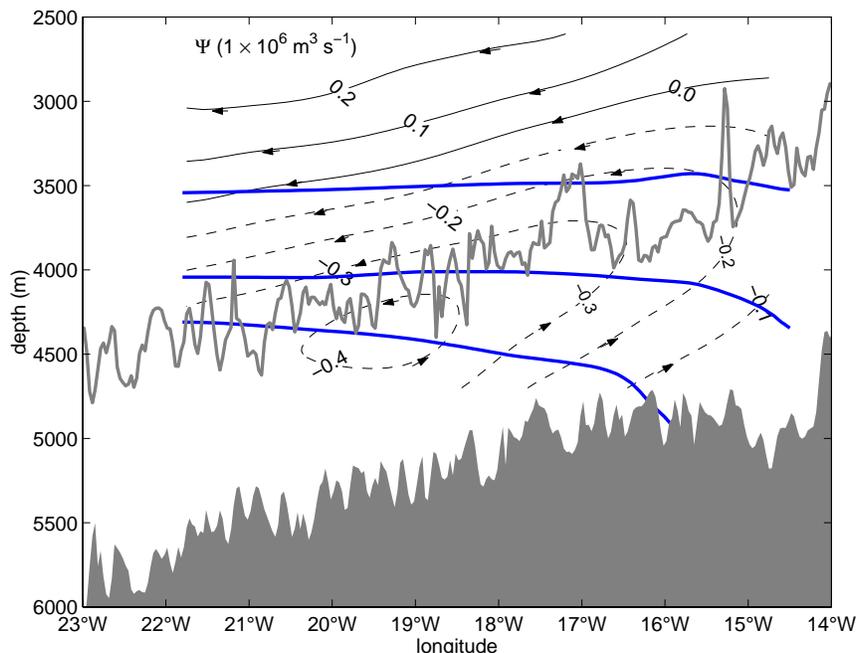
Figure 7. The meridionally integrated stream function as estimated through objective analysis of the inverse model solution. Dimensional values of the stream function are contoured, and uncertainties are roughly ±40%. Representative bathymetry of the canyon floors (shaded) and crests (gray line) is shown, as are the $\sigma_n = 28.10$, 28.16 and 28.20 isopycnals.

Diapycnal upwelling must be occurring in regions where turbulence supports a convergent buoyancy flux: $w_* N^2 \cong -\partial J_b / \partial z > 0$. This condition is satisfied by turbulence occurring close to the bottom, since the buoyancy flux must decrease with depth to meet a no-flux condition at the sea floor. Within the context of (7), the buoyancy flux is related to the dissipation rate by a mixing efficiency parameter, $J_b = -\Gamma \bar{\epsilon}$. We believe that a reduction in mixing efficiency near the bottom allows the no-flux condition to be met at the sea floor. This reduction may occur in a 1 to 10 m thick boundary layer (i.e., the "log layer"), which was unresolved by our measurements. However, variations in mixing efficiency may extend to greater heights in the canyons. The physical mechanisms controlling the efficiency of mixing near topography are not well understood, but turbulent mixing in regions enclosed by topography may favor mixing with reduced efficiency. Stigebrandt and Aure (1989) found that mixing in fjords occurred at 0.05 efficiency. Given our observations of dissipation and stratification along canyon slopes, a decrease in mixing efficiency from 0.2 to 0.05 in the bottom most 100 m above FZ slopes would account for diapycnal upwelling as large as $w_* \cong +300$ m yr^{-1}.

Discussion

We have described buoyancy forcing and circulation occurring in a region of the abyssal ocean. Our calculations suggest that enhanced levels of turbulence above rough bathymetry lead to enhanced levels of diabatic flow. Divergence of the diabatic flow acts as a mechanism of buoyancy forcing for the lateral circulation though the vortex stretching term $(f/h)(w_*(z_u) - w_*(z_l))$ in the vorticity budget. The significance of diabatic vortex stretching as a forcing mechanism must be assessed relative to other forcing agents for the flow. From the inverse estimates, we may compare the strength of buoyancy forcing to the adiabatic mechanism of vortex stretching, represented by $(f/h)\underline{u} \cdot \nabla h$ in the vorticity budget.

Above the level of FZ crests, adiabatic vortex stretching is cyclonic, while diabatic vortex stretching is anticyclonic. In the region where mixing rates are largest, these two mechanisms are comparable in magnitude and the vortex stretching terms in (6) nearly cancel. Since $\beta v \cong 0$, there is little meridional flow just above the level of FZ crests (Fig. 5). The divergence of diapycnal mass flux is clearly a significant forcing agent on the
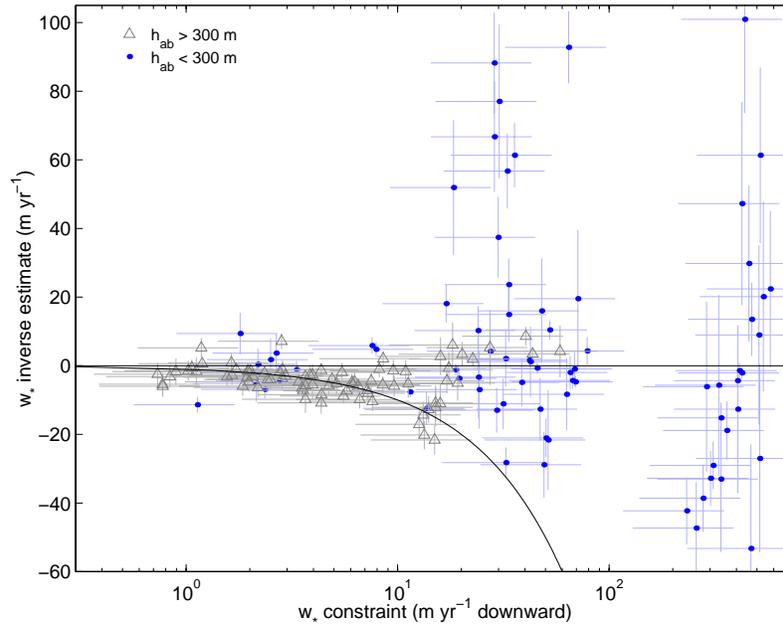
Figure 8. Comparison of the a priori estimates of w_* with the inverse estimates for the $\sigma_n = 28.20$ neutral density surface. Estimates at sites where the $\sigma_n = 28.20$ surface is more than 300 m above the bottom are plotted using triangles, and estimates from sites where $\sigma_n = 28.20$ is less than 300 m above the bottom are plotted as points. The curve along which the inverse and a priori estimates are equal is shown. Standard errors are shown for all estimates.

lateral circulation in this region. Further west of the Mid Atlantic Ridge where mixing rates are weaker, the adiabatic stretching exceeds the diabatic stretching, resulting in the southward flow where the largest lateral velocities occur. In addition to the stretching mechanisms, friction imposed by topography may also be a significant forcing mechanism near the bottom, though we have not attempted to assess this contribution.

The diapycnal advection estimates presented here are clearly sensitive to assumptions made about turbulent mixing efficiency. As indicated by (9), depth variations in mixing efficiency will influence both the magnitude and direction of the diabatic mass flux. We note that most data are consistent with a mixing efficiency R_f near 15% (equivalently, $\Gamma \cong 0.20$). For example, diffusivity estimates from (17), which assume $\Gamma = 0.2 \pm 0.04$ agree with the turbulent diffusivity estimated from the tracer dispersion experiment (*Ledwell et al.*, 2000). Moreover, *St. Laurent et al.* (2001) find general agreement between a priori diapycnal advection estimates estimated with $\Gamma \cong 0.20$ in (18) and diapycnal advection estimates deduced from inversion of the steady-state budgets. Variations in mixing efficiency

are only inferred from estimates deep in FZ canyons, in regions where isopycnal slopes increase as density layers in-crop along the bottom. Our evidence for reduced mixing efficiencies is indirect, but the diapycnal advection estimates are consistent with a reduction from $\Gamma \cong 0.20$ to $\Gamma \cong 0.05$ over a depth of 100 m above the sloping walls of FZ canyons.

While the study strictly considered data from a small geographic region, the bathymetric features present are ubiquitous over the basins of the global ocean, as are the tides. If, as suggested by *Munk and Wunsch* (1998), the tides are the dominant source of mechanical energy for abyssal mixing, the pattern of enhanced turbulence observed over Brazil Basin fracture zones may be representative of turbulence occurring in other regions. Diabatic forcing above rough topography may be a primary forcing mechanism for the abyssal circulation.

References

Alves, M.L.G.R., and A. Colin de Verdiere, Instability dynamics of a subtropical jet and applications to the Azores Front Current System: Eddy-driven mean flow. *J. Phys. Oceanogr., 29*, 837-864, 1999.

Hautala, S.L., and S.C. Riser, A nonconservative β-spiral determination of the deep circulation in the Eastern South Pacific. *J. Phys. Oceanogr., 23*, 1975-2000, 1993.

Hogg, N.G., and W.B. Owens, Direct measurements of the deep circulation within the Brazil Basin. *Deep-Sea Res. II, 46*, 335-353, 1999.

Huq, P., and R.E. Britter, Turbulence evolution and mixing in a two layer stably stratified fluid. *J. Fluid Mech., 285*, 41-67, 1995.

Ivey, G.N., and J. Imberger, On the nature of turbulence in a stratified fluid. Part 1. The energetics of mixing. *J.Phys. Oceanogr., 21*, 650-658, 1991.

Ledwell, J.R., E.T. Montgomery, K.L. Polzin, L.C. St. Laurent, R.W. Schmitt, and J.M. Toole, Mixing over rough topography in the Brazil Basin. *Nature, 403*, 179-182, 2000.

Lozier, S.M.,Evidence for large-scale eddy-driven gyres in the North Atlantic. *Science, 277*, 361-364, 1997.

McDougall, T.J., Thermobaricity, cabbeling, and water-mass conversion. *J. Geophys. Res., 92*, 5448-5464, 1987.

McDougall, T.J., 1Neutral-surface potential vorticity. *Prog. Oceanogr., 20*, 185-221, 1988.

McDougall, T.J., The influence of ocean mixing on the absolute velocity vector. *J. Phys. Oceanogr., 25*, 705-725, 1995.

Moum, J.N., Efficiency of mixing in the main thermocline. *J. Geophys. Res., 101*, 12,057-12,069, 1996.

Munk, W., and C. Wunsch, Abyssal recipes II: energetics of tidal and wind mixing. *Deep-Sea Res. I, 45*, 1977-2010, 1998.

Osborn, T.R., Estimates of the local rate of vertical diffusion from dissipation measurements. *J. Phys. Oceanogr., 10*, 83-89, 1980.

Pedlosky, J., *Ocean Circulation Theory*, Springer-Verlag, 453 pp., 1996.

Polzin, K. L., J.M. Toole, J.R. Ledwell, and R.W. Schmitt, Spatial variability of turbulent mixing in the abyssal ocean. *Science, 276*, 93-96, 1997.

St. Laurent, L.C., J.M. Toole, and R.W. Schmitt, Buoyancy forcing by turbulence above rough topography in the abyssal Brazil Basin. *J. Phys. Oceanogr.*, in press, 2001.

St. Laurent, L., and R.W. Schmitt, The contribution of salt fingers to vertical mixing in the North Atlantic Tracer Release Experiment. *J. Phys. Oceanogr., 24*, 1404-1424, 1999.

Smith, W.H.F., and D.T. Sandwell, Global sea floor topography from satellite altimetry and ship depth soundings. *Science, 277*, 1956-1962, 1997.

Spall, M. A., 1994: Wave-induced abyssal recirculations. *J. Mar. Res., 52*, 1051-1080, 1994.

Spall, M.A., Buoyancy-forced circulations around islands and ridges. *J. Marine. Res., 58*, 957-982, 2000.

Stigebrandt, A., and J. Aure, Vertical mixing in basin waters of fjords. *J. Phys. Oceanogr., 19*, 917-926, 1989.

Stommel, H., The abyssal circulation of the ocean. *Nature, 180*, 733-734, 1957.

Stommel, H., and A.B. Arons, On the abyssal circulation of the World Ocean-I: Stationary planetary flow patterns on a sphere. *Deep-Sea Res., 6*, 140-154, 1960.

Stommel, H. and F. Schott, The beta spiral and the determination of the absolute velocity field from hydrographic station data. *Deep-Sea Res., 24*, 325-329, 1977.